APPLICATION OF HIMAWARI-8 SATELLITE IN THE EVALUATION OF THE FORECASTING PERFORMANCE FOR A WEATHER MODIFICATION MODEL WITHIN CHINA CENTRAL REGION

JIA, W.[1,2] – QIN, M.[3*]

[1]*Weather Modification Centre of Jiangsu Province, No.8, Yushun Rd., Nanjing 210000, China*

[2]*China Meteorological Administration Aerosol-Cloud and Precipitation Key Laboratory, Nanjing University of Information Science and Technology, No.219, Ningliu Rd., Nanjing 210044, China*

[3]*Meteorology Bureau of Yancheng City, No.1, Dongting Rd., Yancheng 224000, China*

[*]*Corresponding author*
e-mail: meiqin740@163.com

(Received 9th Jan 2025; accepted 24th Mar 2025)

Abstract. To address the issues of limited coverage, low spatiotemporal resolution, and insufficient observational data variables in evaluating the forecasting performance of a weather modification model, this study utilized Moderate Resolution Imaging Spectroradiometer (MODIS) polar-orbiting satellite data from September to October 2018. It assessed the reliability of cloud products from the Himawari-8 geostationary satellite, known for its high spatiotemporal resolution and extensive coverage, which was applied to evaluate the forecasting capability of the Cloud and Precipitation Explicit Forecasting System (CPEFS) model in cloud fields over the Central Region of China. The results showed that the spatial distributions of cloud top temperature (CTT) and cloud water path (CWP) observed by Himawari-8 and MODIS were consistent, with monthly average spatial anomaly correlation coefficients (ACC) ranged from 0.51 to 0.67 for CTT and 0.68 to 0.69 for CWP. The average ACC between CPEFS model forecasts and Himawari-8 observations was 0.23 for CTT and 0.34 for CWP. The forecasting performance of CTT exhibited greater variability between cases compared to CWP. Overall, the reliability of forecasts was low at the initial stage, increased with lead time, and then declined in later stages. In higher-performing cases, the early-stage forecasting reliability improved more rapidly.
Keywords: *next-generation geostationary meteorological satellite, cloud observation products, CPEFS model, China Central Region, spatial distribution reliability*

Introduction

Geostationary satellites can remotely sense and retrieve the macro and micro physical characteristic parameters of cloud systems. Compared to the point- or line-based cloud observations from the airborne particle measuring system (PMS), ground-based Global Positioning System (GPS), microwave radiometers, and other instruments, geostationary satellites offer advantages such as a wider observation range and longer observation duration (Ma et al., 2009). Cloud retrieval products are widely used in fields such as meteorology, climatology, environmental studies, and weather modification. The first-generation geostationary satellite Feng Yun-2 (FY-2) launched by China has played a significant role in tracking and understanding the evolution of cloud systems under different dynamic conditions, conducting weather analysis, identifying potential cloud seeding areas, and evaluating the effects of cloud seeding in real-time meteorological services (Zhou et al., 2008).

Japan took the lead in launching the new-generation geostationary satellite of Himawari-8 (Zhang et al., 2016), which is equipped with the 16-channel Advanced Himawari Imager (AHI) developed by the United States. This imager is featured with high-frequency and full-

http://www.aloki.hu ● ISSN 1589 1623 (Print) ● ISSN 1785 0037 (Online)
DOI: http://dx.doi.org/10.15666/aeer/2303_54255441

disk scanning over China Central and Eastern Region. Its imaging time resolution is less than 10 minutes, and its spatial resolution reaches 2 km, making it highly beneficial for observing and early warning of severe convective weather, as well as for verifying the forecasting performance of cloud-resolution weather modification models. Specifically, the near-real-time retrieval processing system of Fengyun Geostationary Algorithm Testing Platform (FYGAT) provides a wealth of cloud products (Min et al., 2017), such as cloud top height/temperature, cloud water path, and cloud phase, which can be used to assess the forecasting performance of weather modification models for both macro and micro cloud features (Liu et al., 2021).

Geostationary satellites often use passive remote sensing techniques to retrieve cloud characteristic parameters, offering a wide range of products and diverse algorithms. In the 1970s, scientists proposed the retrieval algorithm of cloud top height based on a single infrared window (Fan et al., 2017), but Nieman et al. (1993) found significant discrepancies. Shenk and Curran (1973) introduced the method of solar reflectance and infrared window to reduce errors. Szejwach (1982) used the H_2O absorption channel and infrared window channel to retrieve cloud top brightness temperature, yielding results closer to the temperature at cloud top height. Hamada et al. (2008) proposed the lookup table method of infrared split-window, with the estimation errors of cloud top height under 1 km. Smith and Frey (1990) introduced the radiative ratio method, which matched well with lidar results. Regarding cloud optical thickness and effective particle radius, Szejwach developed an algorithm for retrieving cirrus cloud optical thickness and the average effective ice particle size using infrared channels, while Zhao et al. (2002), Zhou et al. (2008), and others in China researched multi-channel retrieval algorithms of cloud optical thickness using Fengyun satellite data, achieving good results. For cloud phase retrieval, Ackerman found that on the scatter plot of brightness temperature difference between 8-11 μm and 11-12 μm channel, ice clouds had a slope greater than 1, water clouds less than 1, and mixed-phase clouds near 1, which was applied by the Moderate Resolution Imaging Spectroradiometer (MODIS) for cloud phase identification (Ackerman et al., 1999). However, since retrieval products are not direct observations and some algorithms are affected by region, season, and satellite viewing angles, understanding the reliability of the products is essential before application.

The Himawari-8 satellite, as the prototype for the next-generation U.S. geostationary meteorological satellites, had its operational applications in Japan primarily based on the inherited retrieval algorithms from the United States. Cloud product verification was also carried out using the same MODIS-based algorithm (Mouri et al., 2016). China has integrated the Himawari-8 satellite data into FYGAT (Wang et al., 2019), and developed a near-real-time processing system for scientific products of the Himawari-8 satellite. This system aimed to more effectively utilize the Himawari-8 data to serve China's meteorological service, while also further testing the product algorithms for the FY-4 satellite. The goal was to continuously improve the algorithms through product application and feedback. This study planned to utilize MODIS retrieval cloud products to analyze the reliability of the Himawari-8 satellite's cloud products for different cloud systems over China Central Region.

The main application areas of the Himawari-8 satellite in China include short-term forecasting and environmental forecasting, with relatively fewer applications in artificial weather modification. The MODIS cloud products were an important basis for analyzing the macro- and micro-physical characteristics of cloud systems, but they can only achieve global atmospheric coverage once every 1-2 days, resulting in the limited temporal and spatial coverage. To achieve the transition of weather modification model forecast verification from case studies to real-time operational applications, the FY-2 geostationary satellite data was

http://www.aloki.hu ● ISSN 1589 1623 (Print) ● ISSN 1785 0037 (Online)
DOI: http://dx.doi.org/10.15666/aeer/2303_54255441

primarily applied in quantitative verification of weather modification models (Zhang et al., 2018; Li et al., 2020; Mei et al., 2022). FY-2 geostationary satellite data is suitable for the real-time operational verification in weather modification models in quantities, due to its significant wider time-spatial coverage than MODIS orbit satellite. However, the first-generation geostationary satellite of FY-2 with limited 5-channel and low spatial resolution of 5 km is not suitable spatial-refined and cloud-element-diversified evaluation of weather modification model. In contrast, the new-generation Himawari-8 geostationary meteorological satellite is equipped with an advanced 16-channel AHI, improving the spatial resolution to 2 km and offering full-disk rapid scanning capabilities with a temporal resolution as high as 10 minutes. This effectively meets the real-time demands of meteorological operations. Moreover, the cloud product retrieval uses the improved algorithm of FYGAT which could produce more cloud element fields. Therefore, this study aimed to use the new-generation Himawari-8 satellite, which offers high spatiotemporal resolution and wide coverage, to address issues in real-time operational verification of weather modification models, such as the low spatiotemporal resolution of observational data and the singularity of observation products.

Materials and methods

The study firstly evaluated the reliability of cloud products from the Himawari-8 geostationary satellite over China Central Region using the MODIS polar-orbiting satellite observation data. Based on this evaluation, the products of cloud top temperature (CTT) and cloud water path (CWP) from the Himawari-8 satellite with high reliability was used to validate the forecasting performance of the Cloud and Precipitation Explicit Forecasting System (CPEFS) model in cloud field over China Central Region. The CPEFS model, built on the WRF Version 3.5 model as its dynamic framework, couples the cloud-precipitation explicit scheme of China Academy of Meteorological Science (CAMS) developed by the Weather Modification Center of the China Meteorological Administration. It generates forecast products of cloud field twice daily at 00 and 12 UTC. The products feature a horizontal resolution of 3 km, 19 vertical layers, and a forecast range of up to 48 hours.

Firstly, 26 non-continuous and hourly overpass observations of cloud top temperature and cloud water path with 1 km or 5 km resolution from the MODIS polar-orbiting satellite over China Central Region (107.5-123.5ºE, 28.5-38.5ºN) in September and October 2018 were selected (*Table 1*). The spatial anomaly correlation coefficient (ACC) was used to compare and analyze the spatial distribution similarity of cloud field between the Himawari-8 geostationary satellite observations with 4 km resolution and the MODIS satellite observations with 1 km or 5 km resolution. The specific formula is as follows:

$$\mathbf{ACC} = \frac{\frac{1}{n}\sum_{k=1}^{n}(S_{m,k}-\overline{S_m})(S_{h,k}-\overline{S_h})}{\sqrt{\frac{1}{n}\sum_{k=1}^{n}(S_{m,k}-\overline{S_m})^2}\sqrt{\frac{1}{n}\sum_{k=1}^{n}(S_{h,k}-\overline{S_h})^2}} \quad \text{(Eq.1)}$$

where $S_{m,k}$ and $S_{h,k}$ represent the variable values at the k-th grid point for MODIS and Himawari-8, respectively. Where $\overline{S_m}$ and $\overline{S_h}$ represent the spatial average of the variable values from MODIS and Himawari-8, respectively. n is the number of grid points in the study area. The value of ACC ranges from -1 to 1, with a higher ACC indicating higher CTT or CWP spatial distribution similarity between Himawari-8 and MODIS satellite.

http://www.aloki.hu ● ISSN 1589 1623 (Print) ● ISSN 1785 0037 (Online)
DOI: http://dx.doi.org/10.15666/aeer/2303_54255441

This suggests that the spatial distribution of cloud products from Himawari-8 is more similar to that of MODIS.

Table 1. *Observational times of the MODIS polar-orbiting satellite over China Central Region in September-October 2018 (UTC)*

	September	**October**
Observational Times	18 UTC on the 4th	01 UTC on the 4th
	05 UTC on the 5th	18 UTC on the 6th
	03 UTC on the 9th	05 UTC on the 7th
	14 UTC on the 9th	03 UTC on the 11th
	19 UTC on the 10th	14 UTC on the 11th
	04 UTC on the 15th	19 UTC on the 12th
	15 UTC on the 15th	06 UTC on the 13th
	18 UTC on the 20th	15 UTC on the 17th
	05 UTC on the 21th	18 UTC on the 22th
	03 UTC on the 25th	05 UTC on the 23th
	14 UTC on the 25th	03 UTC on the 27th
	19 UTC on the 26th	14 UTC on the 27th
	06 UTC on the 27th	06 UTC on the 29th

Subsequently, the 3 km resolution forecasts from the CPEFS model and the 4 km resolution observations from the Himawari-8 satellite were interpolated onto the 6 km resolution grid of the CPEFS model. Using the spatial ACC, a comprehensive evaluation was conducted on the performance of the spatial distributions of cloud top temperature and cloud water path forecasted by the CPEFS model initialized at 00 and 12 UTC for eight precipitation weather events (represented by 0904, 0919, 0921, 0922, 0923, 0924, 1012, and 1021) over China Central Region during September and October 2018. The synoptic conditions of these events in September were related to the low-pressure trough in the westerly belt and Western Pacific Subtropical High, with convective and stratiform mixed clouds. The synoptic conditions of these events in October were related to the low-pressure trough in the westerly belt and southwest warm and humid airflow from the Bay of Bengal, with the stratiform clouds. The above convective and stratiform mixed clouds and stratiform clouds with supercooled water were the optimal target clouds for artificial precipitation stimulation in autumn over the research region.

Results

Reliability of the cloud products from Himawari-8 satellite

Cloud top temperature

As shown in *Figure 1*, the spatial ACC of cloud top temperature between the MODIS observations with resolutions of 1 km or 5 km and the Himawari-8 observations with a resolution of 4 km over China Central Region during September and October 2018 were presented. The monthly average ACC ranged from 0.51 to 0.67. Specifically, the ACC between the MODIS 5 km resolution observations and the Himawari-8 4 km resolution observations ranged from 0.61 to 0.67, while those between the MODIS 1 km resolution observations and the Himawari-8 observations ranged from 0.51 to 0.61. The MODIS 5 km resolution observations demonstrated the better spatial consistency with the Himawari-8 observations. Using the MODIS 5 km resolution observations as a reference,

http://www.aloki.hu ● ISSN 1589 1623 (Print) ● ISSN 1785 0037 (Online)
DOI: http://dx.doi.org/10.15666/aeer/2303_54255441

the average ACC between the MODIS and the Himawari-8 observations was 0.67 in September and 0.61 in October. The Himawari-8 observations in September showed approximately 10% higher agreement with the MODIS compared to the results in October.

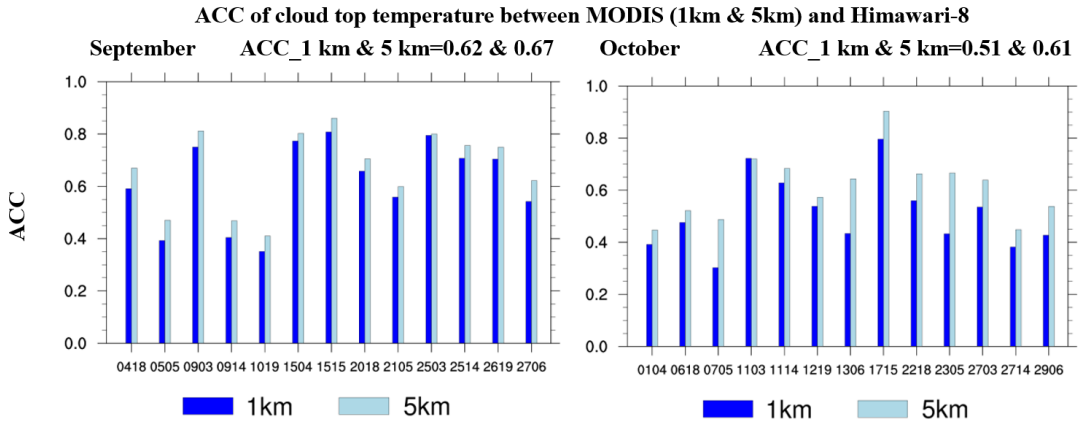

Figure 1. *The spatial anomaly correlation coefficients (ACC) of cloud top temperature with resolutions of 1 km or 5 km from MODIS and Himawari-8 satellite over China Central Region during September (left) and October (right) 2018 (X-axis: the first two digits represent the observation date, and the last two digits represent the observation time. ACC_1 km and ACC_5 km denote the monthly average ACC for 1 km and 5 km resolutions, respectively)*

As shown in *Figure 1 (left)*, a total of 13 hourly MODIS observations over China Central Region during September were analyzed for the spatial correlation with the Himawari-8 observations. The maximum ACC reached 0.85 at 15 UTC on September 15, while the minimum was 0.40 at 19 UTC on September 10. As illustrated in *Figure 2 (top)*, MODIS observations indicated that at 15 UTC on September 15, a cloud system covered the southwestern part of China Central Region. Predominantly aligned along a southwest-northeast axis, the cloud system exhibited a spatial pattern of lower cloud top in the middle and higher on both sides. The central area was mostly cloud-free or covered by warm clouds, with cloud top temperature above 273 K. Moving northward, the cloud cover increased, and cloud top temperature decreased to below 273 K, indicating cold clouds. In the southern part, localized areas of higher cold clouds were observed, with minimum cloud top temperature below 230 K. Compared with the MODIS, the Himawari-8 offered broader observation coverage across China Central Region. The Himawari-8 observations showed a similar spatial pattern of cloud-free and high-low cloud distributions aligned along a southwest-northeast axis, compared with the MODIS results. As shown in *Figure 2 (middle)*, the MODIS observation results at 19 UTC on September 10 revealed the cloud coverage in the western part of China Central Region. Predominantly aligned along a south-north axis, the spatial pattern featured higher cloud top in the west and lower in the east. The western area consisted of cold clouds with cloud top temperature below 273 K, dropping to a minimum below 230 K, while the eastern area was covered by warm clouds or cloud-free, with cloud top temperature exceeding 273 K. In contrast, due to data gaps, the Himawari-8 failed to effectively observe warm clouds in the western part of China Central Region and did not capture the spatial distribution of cold and warm clouds well, resulting in a relatively low spatial ACC with the MODIS. As shown in *Figure 2 (bottom)*, the observations at 03 UTC on September

http://www.aloki.hu ● ISSN 1589 1623 (Print) ● ISSN 1785 0037 (Online)
DOI: http://dx.doi.org/10.15666/aeer/2303_54255441

25, when the MODIS and Himawari-8 both effectively covered the entire region with minimal data gaps, revealed a spatial ACC of 0.80. The observation results were consistent, successfully identifying extensive cold cloud coverage across China Central Region, except for the southeastern corner. Additionally, a hammer-shaped shallow cold cloud structure was observed in the western area.

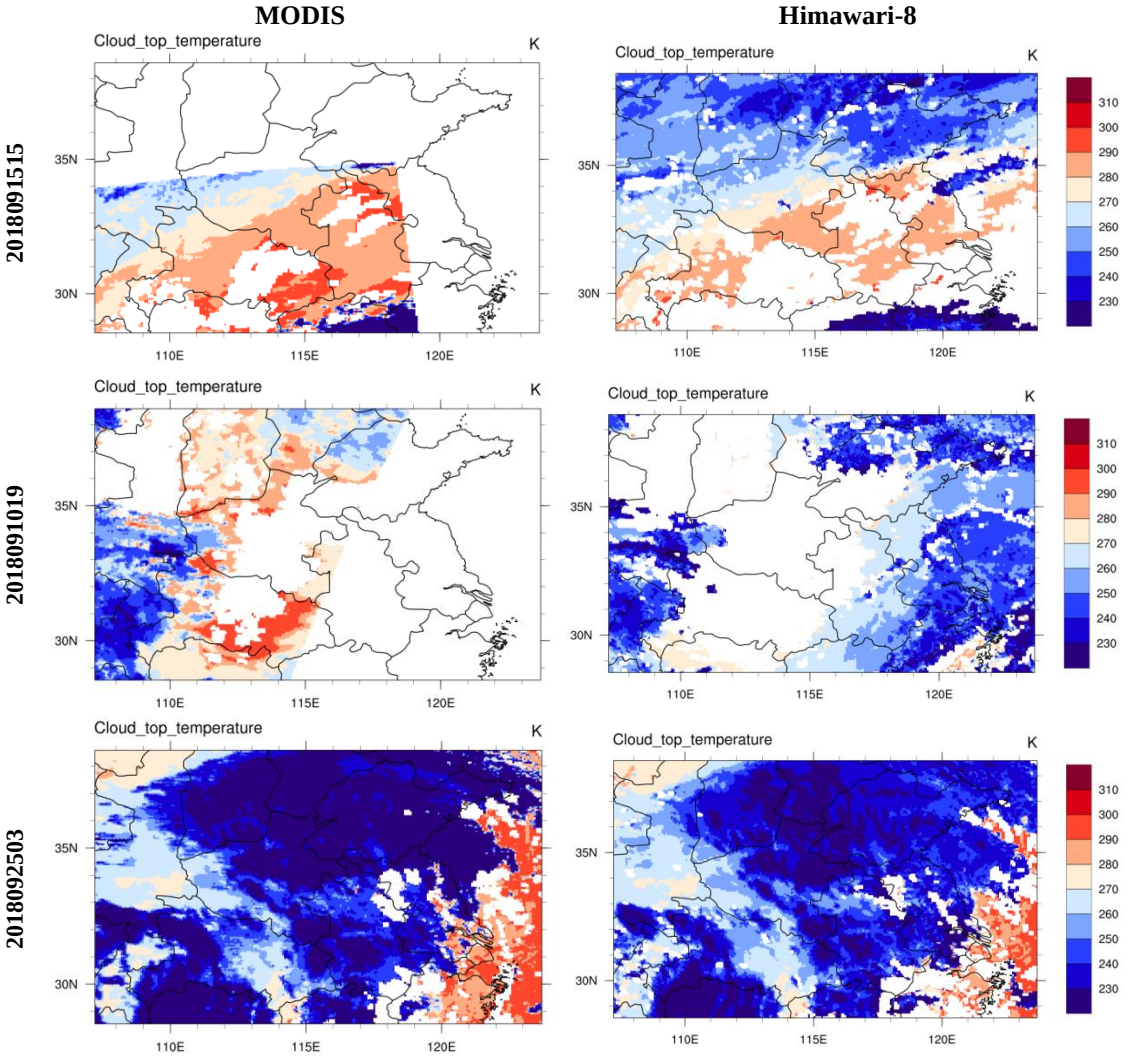

Figure 2. *Comparison of cloud top temperature observations over China Central Region from the MODIS and Himawari-8 satellite at 15 UTC on September 15, 19 UTC on September 10, and 03 UTC on September 25, 2018 (blank areas indicate cloud-free regions or missing data)*

As shown in *Figure 1 (right)*, a total of 13 hourly MODIS observations over China Central Region during October were analyzed for the spatial correlation with the Himawari-8 observations. The maximum ACC reached 0.90 at 15 Coordinated Universal Time (UTC) on October 17. As illustrated in *Figure 3 (top)*, the MODIS observations at 15 UTC on October 17 indicated cloud coverage in the southwestern part of China Central Region, with cloud top temperature around 273 K, consistent with the Himawari-8 observations. As shown in *Figure 3 (bottom)*, the observations at 06 UTC on October 13, when the MODIS and Himawari-8 both effectively covered the entire region with

http://www.aloki.hu ● ISSN 1589 1623 (Print) ● ISSN 1785 0037 (Online)
DOI: http://dx.doi.org/10.15666/aeer/2303_54255441

minimal data gaps, revealed a spatial ACC of 0.65. The observation results successfully identified extensive cold cloud coverage across China Central Region, except for the northeastern corner, with localized shallow cold clouds observed in the southwestern part.

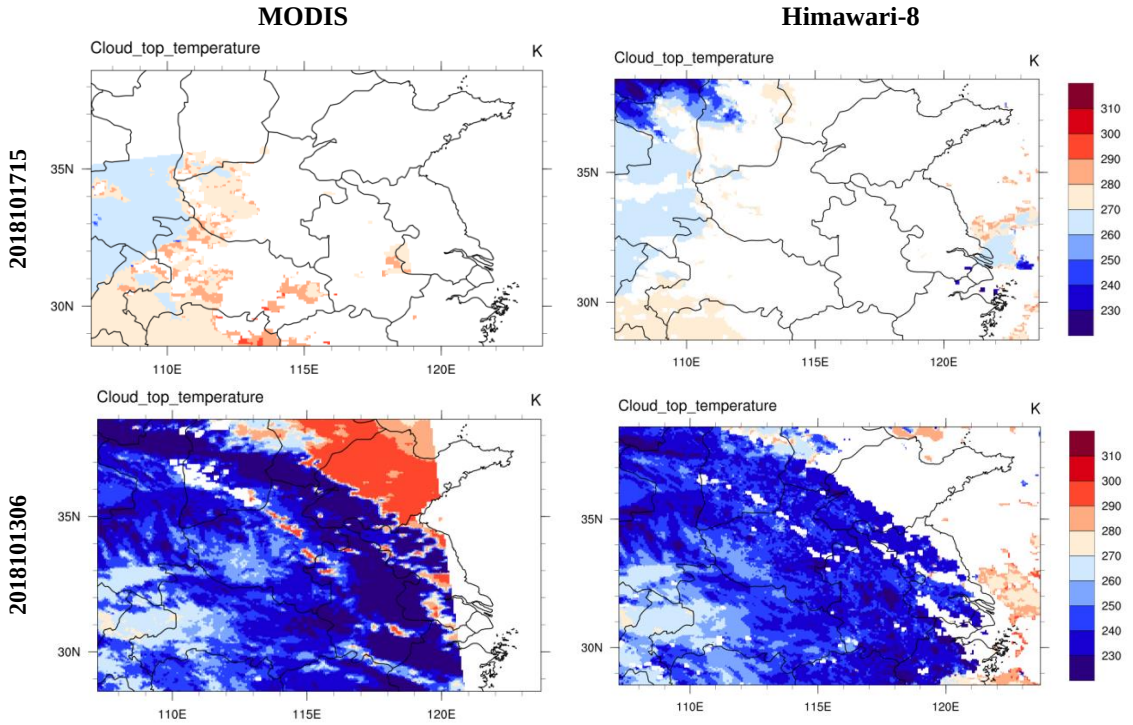

Figure 3. *Comparison of cloud top temperature observations over China Central Region from the MODIS and Himawari-8 satellite at 15 UTC on October 17, and 06 UTC on October 13, 2018 (blank areas indicate cloud-free regions or missing data)*

Cloud water path

The cloud water path is retrieved using microphysical parameters, including daytime cloud optical thickness and cloud particle effective radius. The satellite observation sample size for cloud water path is smaller than that for cloud-top temperature, and only products with a resolution of 1 km are available. *Figure 4* presented the spatial ACC of cloud water path between MODIS observations with the 1 km resolution and Himawari-8 observations with the 4 km resolution over China Central Region in September and October 2018. The monthly average ACC ranged from 0.68 to 0.69, with minimal differences in accuracy between September and October.

As shown in *Figure 4 (left)*, a total of 6 hourly MODIS observations over China Central Region during September were analyzed for the spatial correlation with the Himawari-8 observations. The maximum ACC reached 0.80 at 03 UTC on September 9, while the minimum ACC was 0.60 at 05 UTC on September 5. As shown in the upper part of *Figure 5*, the MODIS observations indicated that at 03 UTC on September 9, there was relatively abundant cloud water content in the northwestern part of China Central Region, with values exceeding 200 g/m², which was consistent with the spatial distribution observed by Himawari-8. As shown in the lower part of *Figure 5*, the MODIS observations indicated that at 05 UTC on September 5, there was abundant cloud water in the central and western region of China Central Region, with values greater than

http://www.aloki.hu ● ISSN 1589 1623 (Print) ● ISSN 1785 0037 (Online)
DOI: http://dx.doi.org/10.15666/aeer/2303_54255441

200 g/m². The Himawari-8 effectively detected this cloud water-rich region, but the range of cloud water content greater than 700 g/m² was significantly smaller than the MODIS observations, and there were spatial distribution differences, which led to a decrease in the ACC to 0.6.

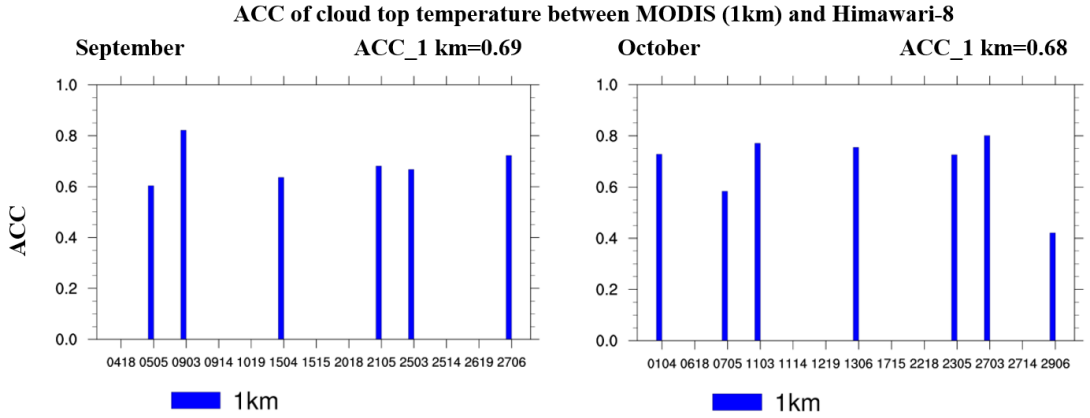

Figure 4. *The spatial anomaly correlation coefficients (ACC) of cloud water path with resolution of 1 km from the MODIS and Himawari-8 satellite over China Central Region during September (left) and October (right) 2018 (X-axis, the first two digits represent the observation date, and the last two digits represent the observation time. ACC_1 km denote the monthly average ACC for 1 km resolution)*

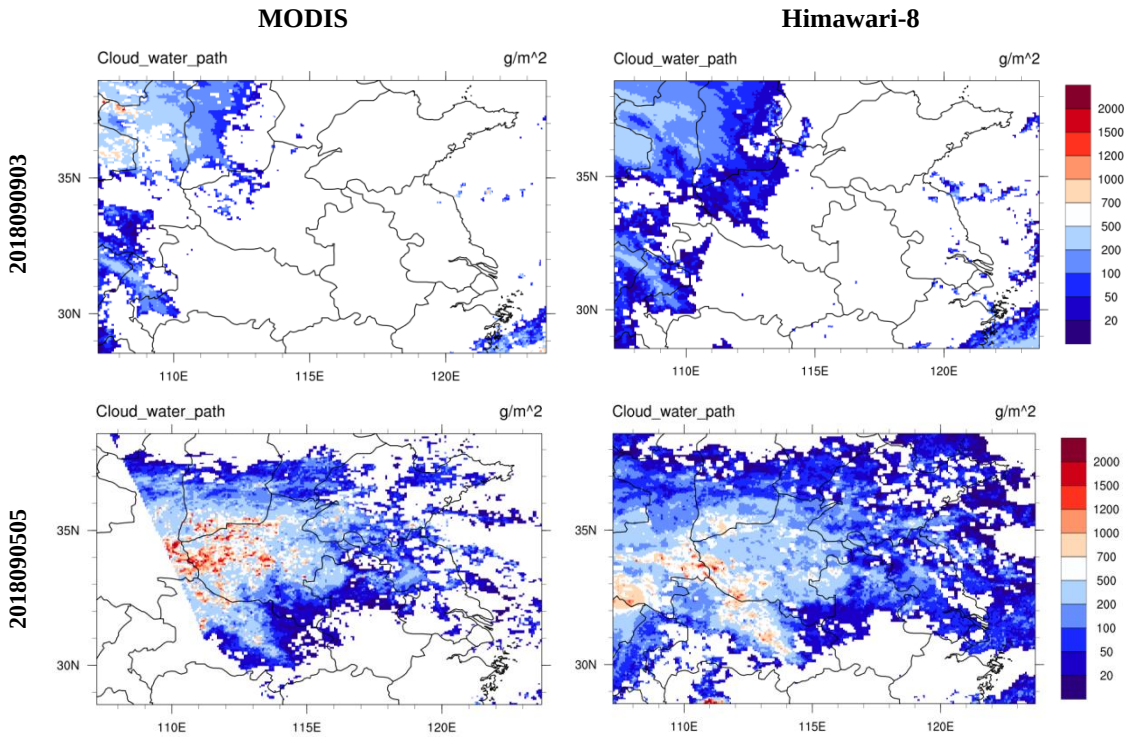

Figure 5. *Comparison of cloud water path observations over China Central Region from the MODIS and Himawari-8 satellite at 03 UTC on September 9, and 05 UTC on September 5, 2018 (blank areas indicate cloud-free regions or missing data)*

http://www.aloki.hu ● ISSN 1589 1623 (Print) ● ISSN 1785 0037 (Online)
DOI: http://dx.doi.org/10.15666/aeer/2303_54255441

As shown in *Figure 4 (right)*, a total of 7 hourly MODIS observations over China Central Region during October were analyzed for the spatial correlation with the Himawari-8 observations. The maximum ACC reached 0.80 at 03 UTC on October 27, while the minimum ACC was 0.40 at 06 UTC on October 29. As shown in the upper part of *Figure 6*, the MODIS observations indicated that at 03 UTC on October 27, there was relatively abundant cloud water content in the southwest corner of China Central Region, consistent with the spatial distribution observed by the Himawari-8. In the middle part of *Figure 6*, the MODIS observations indicated that at 06 UTC on October 29, there was sporadic cloud water in the southwest corner of China Central Region. The Himawari-8 effectively detected this cloud water resource, but the observed area was larger than that of the MODIS, leading to a smaller ACC. The cloud water resources over China Central Region in October were significantly lower than in September.

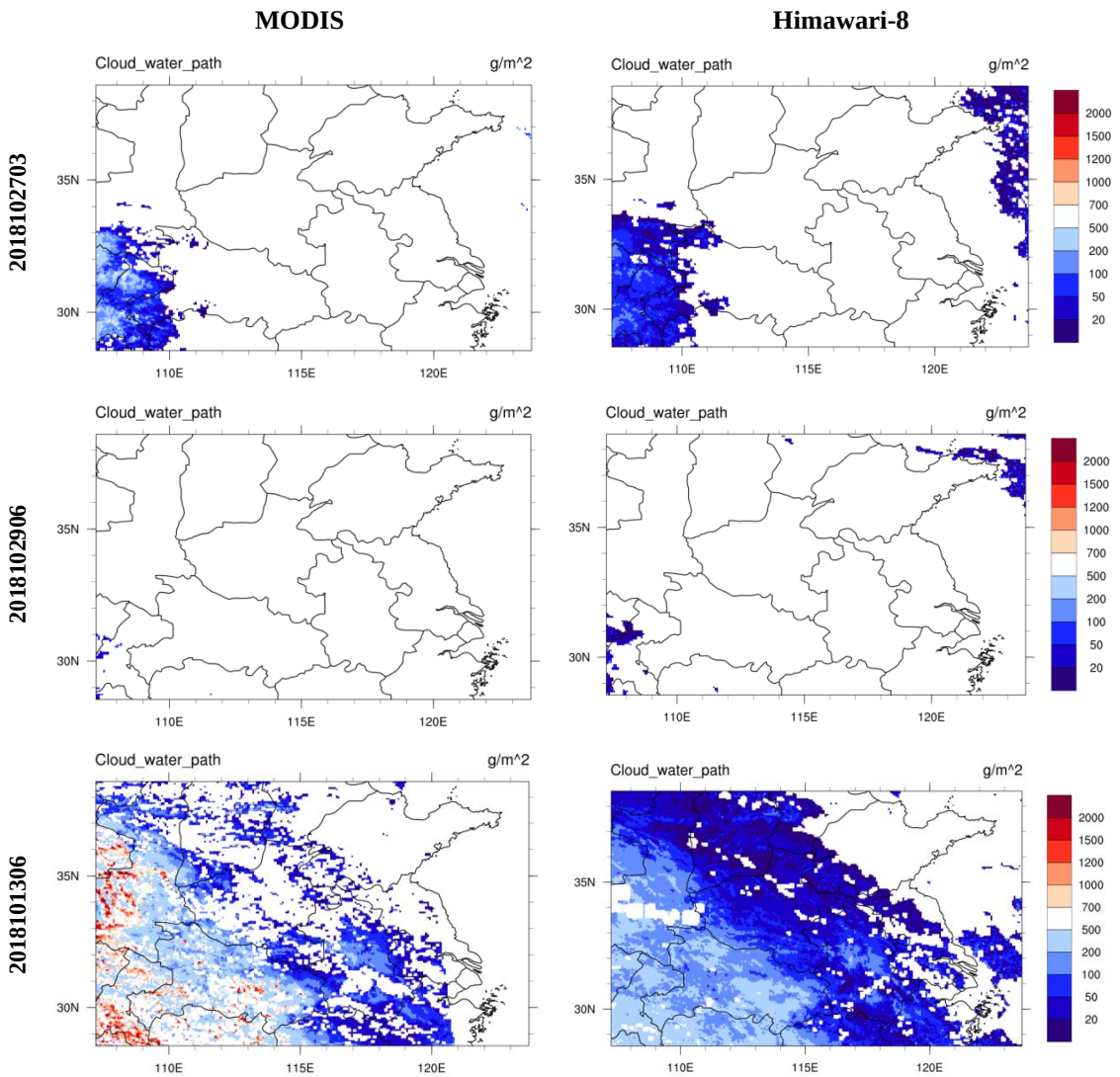

Figure 6. *Comparison of cloud water path observations over China Central Region from the MODIS and Himawari-8 satellite at 03 UTC on October 27, 06 UTC on October 29, and 06 UTC on October 13, 2018 (blank areas indicate cloud-free regions or missing data)*

http://www.aloki.hu ● ISSN 1589 1623 (Print) ● ISSN 1785 0037 (Online)
DOI: http://dx.doi.org/10.15666/aeer/2303_54255441

The lower part of *Figure 6* showed the simultaneous effective coverage of the entire region by both the MODIS and Himawari-8 at 06 UTC on October 13, with large-scale cloud water resources. The spatial ACC reached 0.75, indicating a good match between the observed results from the MODIS and Himawari-8, which effectively detected the decreasing distribution trend of cloud water content from southwest to northeast across China Central Region.

Performance evaluation of CPEFS model based on Himawari-8 satellite

The products of cloud water path and cloud top temperature from the Himawari-8 satellite, after being compared and analyzed for the accuracy against MODIS observations, were used to quantitatively assess the forecasting performance of the new-generation weather modification model of CPEFS during eight precipitation weather events from September to October 2018 initialized at 00 and 12 UTC. *Table 2* presented the average spatial ACC of CWP and CTT betweed the CPEFS forcasts and the Himawari-8 satellite observations for individual cases, which were 0.34 and 0.23, respectively. This indicated that the model forecasts for the spatial distribution of cloud water path were better than that for the cloud top temperature. Overall, the forecasts initialized at 12 UTC showed slightly better results than the forecasts initialized at 00 UTC.

Table 2. *The ACC of Cloud water path and cloud top temperature between the Himawari-8 observations and the CPEFS model forecasts initialized at 00 UTC (S00) and 12 UTC (S12)*

	Cloud Water Path			**Cloud Top Temperature**		
ACC	S00	S12	average	S00	S12	average
	0.32	0.35	0.34	0.21	0.24	0.23

Cloud top temperature

The cloud top temperature reflects the macroscopic development characteristics of the cloud system and is also an important reference for selecting the cloud height in cloud seeding for cold clouds. The left side of *Figure 7* showed the spatial similarity between the cloud top temperature forecasted by the CPEFS model and the Himawari-8 observations for 8 days. The spatial ACC for different cases ranged from 0.05 to 0.6, with significant differences. On September 19, 22-23, and October 21, the ACC were relatively high, while on September 4, 21, and 24, the ACC were relatively low. As shown in the upper part of *Figure 8*, the cloud top temperature forecasted by the CPEFS model initialized at 12 UTC on September 23 in 2018 closely matched the Himawari-8 observations. The model predicted the convective clouds and their distribution in terms of depth and spatial nonuniformity in the southwest part of China Central Region quite well.

The left side of *Figure 9* showed the time series of spatial similarity between the cloud top temperature forecasted by the CPEFS model initialized at 00 UTC and the Himawari-8 observations for cases of relatively good and poor performance with lead time. The spatial ACC between the 3-hour forecasted cloud top temperature and the Himawari-8 observations ranged from 0 to 0.6, with significant differences between individual cases. For better-performing cases, the adjustment at the start of the forecast was relatively quick, and the spatial ACC of cloud top temperature reached 0.6, such as on October 21.

http://www.aloki.hu ● ISSN 1589 1623 (Print) ● ISSN 1785 0037 (Online)
DOI: http://dx.doi.org/10.15666/aeer/2303_54255441

For poorer-performing cases, the adjustment at the start of the forecast was much slower, and the spatial ACC of cloud top temperature is only 0, such as on September 21. As the forecast lead time increased, the spatial similarity between the forecasted and Himawari-8 cloud top temperature for better-performing cases steadily improved, while for poorer-performing cases the spatial similarity significantly decreased.

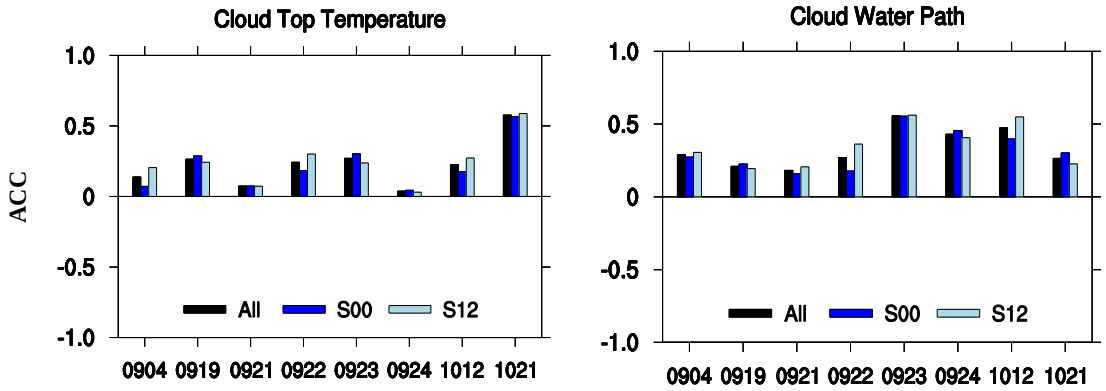

Figure 7. *The average ACC of cloud top temperature (left) and cloud water path (right) within 48-hour forecast for different cases initialized at 00 and 12 UTC over 8 days between the CPEFS model forecasts and the Himawari-8 observations (X-axis: first two digits represent the month and last two digits represent the date of the case. S00 and S12 indicate cases initialized at 00 and 12 UTC, All represents the average ACC of S00 and S12)*

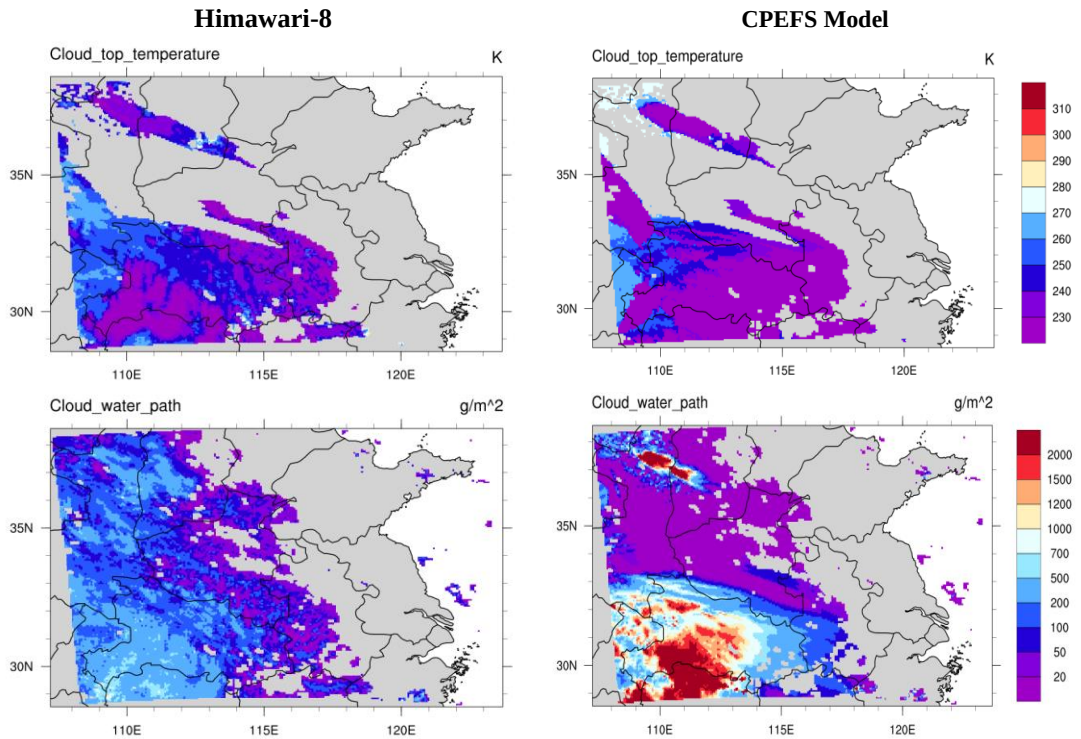

Figure 8. *Comparison of the 18th hour forecasts (right) of cloud top temperature (top) and cloud water path (bottom) for case 0923 initialized at 12 UTC with the Himawari-8 observations (left)*

http://www.aloki.hu ● ISSN 1589 1623 (Print) ● ISSN 1785 0037 (Online)
DOI: http://dx.doi.org/10.15666/aeer/2303_54255441

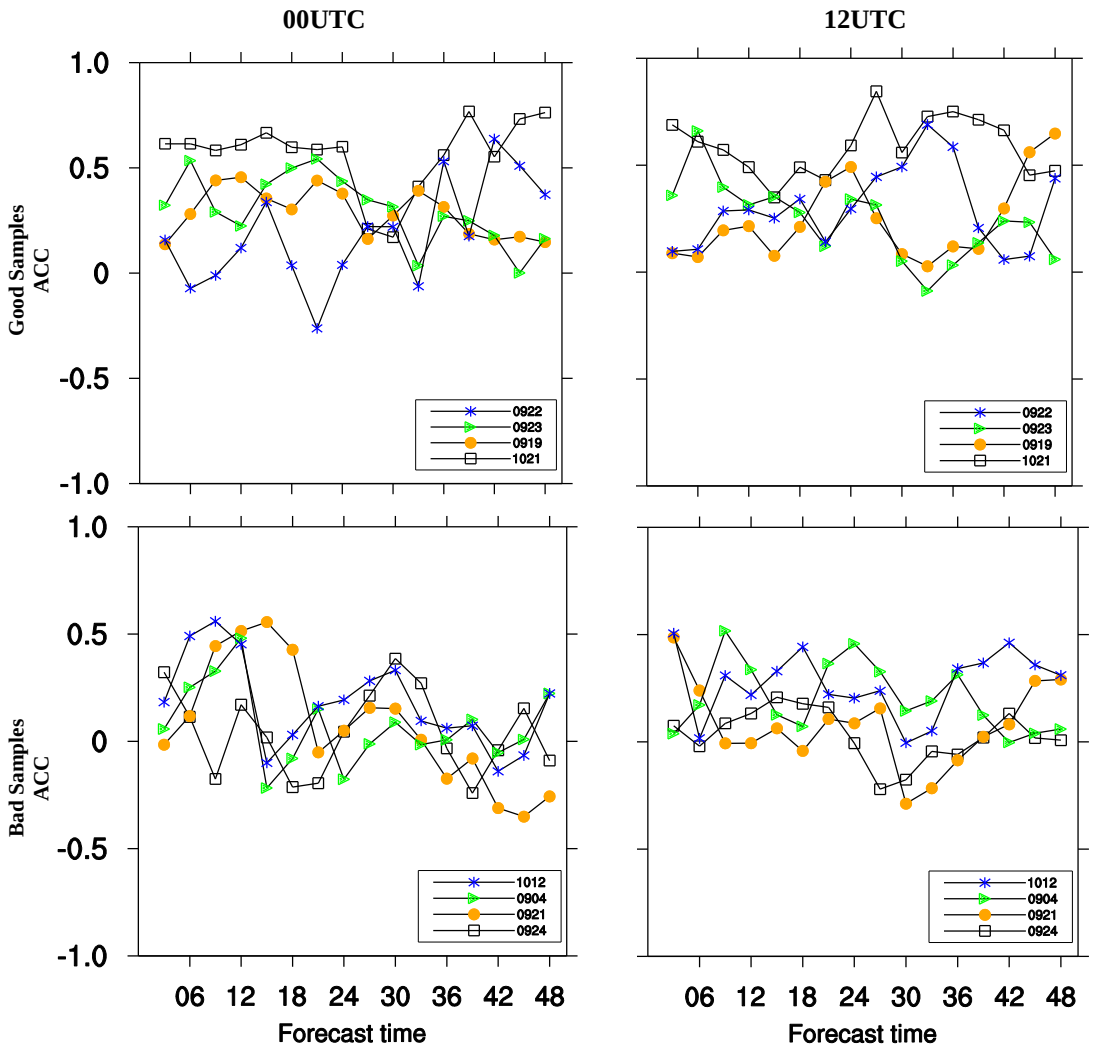

Figure 9. *Time series of the spatial ACC of cloud top temperature between the CPEFS model forecasts initialized at 00 (left) /12 (right) UTC and the Himawari-8 observations for cases of good samples (top) and bad samples (bottom) in performance with the forecast lead time*

The right side of *Figure 9* presented the time series of spatial similarity between the cloud top temperature forecasted by the CPEFS model initialized at 12 UTC and the Himawari-8 observations for cases of relatively good and poor performance with lead time. The 3-hour cloud top temperature forecast of the model showed a spatial ACC with the observed values ranging from 0 to 0.7. The differences in the spatial ACC among different cases were more pronounced. For the better-performing cases, the adjustment during the forecast initiation phase was rapid, and the spatial ACC of cloud top temperature reached 0.7, as seen on October 21. In contrast, for the worse-performing cases, the adjustment during the forecast initiation phase was slow, with a spatial ACC of only 0, as seen on September 4. As the forecast lead time increased, the spatial similarity between the cloud top temperature forecasts and the Himawari-8 observations in the better-performing cases steadily improved, while in the worse-performing cases the spatial similarity significantly decreased.

http://www.aloki.hu ● ISSN 1589 1623 (Print) ● ISSN 1785 0037 (Online)
DOI: http://dx.doi.org/10.15666/aeer/2303_54255441

Cloud water path

Cloud water path represents the total amount of cloud water in the atmosphere, which is the direct source of surface precipitation and also the largest potential for cloud seeding operations. It is essential to evaluate the model's performance in forecasting the cloud water path. However, retrieving this variable value requires microphysical parameters such as daytime cloud optical thickness and effective radius of cloud particles. As a result, the frequency of cloud water path observations by the Himawari-8 satellite is significantly lower compared to other cloud variable. The right side of *Figure 7* showed the spatial similarity between the cloud water path forecasts by the CPEFS model and the Himawari-8 observations for eight days. The spatial ACC for different cases ranged from 0.15 to 0.55. The ACC were relatively high for September 23–24 and October 12, while they were lower for September 4, 19, 21, and October 21. Overall, the spatial similarity between the forecast of cloud water path initialized at 12 UTC and the Himawari-8 observation was higher than that of the forecast initialized at 00 UTC. On September 4, 23, 24, and October 12, the spatial ACC of cloud water path with the observations for the forecast initialized at 12 UTC was higher than for the forecast initialized at 00 UTC, with the largest difference in the ACC being 0.15. As shown in the lower part of *Figure 8*, the forecast of cloud water path by the CPEFS model initilaized at 12 UTC on September 23 in 2018, closely matched the Himawari-8 observations. The model accurately predicted the regions of abundant cloud water in the southwestern, northwestern, and southeastern corners of China Central Region.

The left side of *Figure 10* presented the time series of spatial similarity between the cloud water path predicted by the 00 UTC initialization of the CPEFS model and the Himawari-8 observations for relatively better and poorer cases. The spatial ACC between the model-predicted cloud water path and observations during the 3-6 h forecast period was generally low, ranging from 0 to 0.5. This discrepancy may be attributed to the model's adjustment process in the initial phase, involving the coordination of various physical variable related to atmospheric cloud water resources, resulting in lower agreement with observations. Moreover, significant differences existed in the ACC among individual cases. For better cases, the model adjusted rapidly during the initialization phase, achieving spatial ACC of 0.4-0.5 with observed cloud water path, as seen on September 23-24. In contrast, for poorer cases, the adjustment was much slower, with the ACC as low as 0-0.1, as seen on September 21-22. As the forecast progressed, the spatial similarity between the predicted and observed cloud water path increased rapidly during the 33-36h forecast period. The improvement was particularly pronounced for better cases, with the maximum ACC reaching 0.75, as seen on September 23. In contrast, the increase for poorer cases was relatively slower. Therefore, overall, the reliability of the cloud water path predictions initialized at 00 UTC during the initial phase was low, and its stability required further improvement.

The right side of *Figure 10* presented the time series of spatial similarity between the cloud water path predicted by the 12 UTC initialization of the CPEFS model and the Himawari-8 observations for relatively better and poorer cases. During the 15-18 h forecast period, the spatial similarity between the model-predicted cloud water path and Himawari-8 observations was generally higher, with the ACC ranging from 0.1 to 0.7. After more than 10 hours of coordinated adjustments among various physical variable of atmospheric cloud water resources, most model-predicted cloud water path aligned better with observations. However, significant differences between individual cases persisted. For better cases, the model adjusted quickly during the initialization phase, achieving a

http://www.aloki.hu ● ISSN 1589 1623 (Print) ● ISSN 1785 0037 (Online)
DOI: http://dx.doi.org/10.15666/aeer/2303_54255441

maximum spatial ACC of 0.7 with the Himawari-8 observations, as seen on September 23. Conversely, for poorer cases, the adjustment remained slow, with the ACC as low as 0.1, as seen on September 19. As the forecast progressed, the spatial similarity between the predicted and observed cloud water path during the 39-42 h forecast period showed an overall declining trend for the better cases.

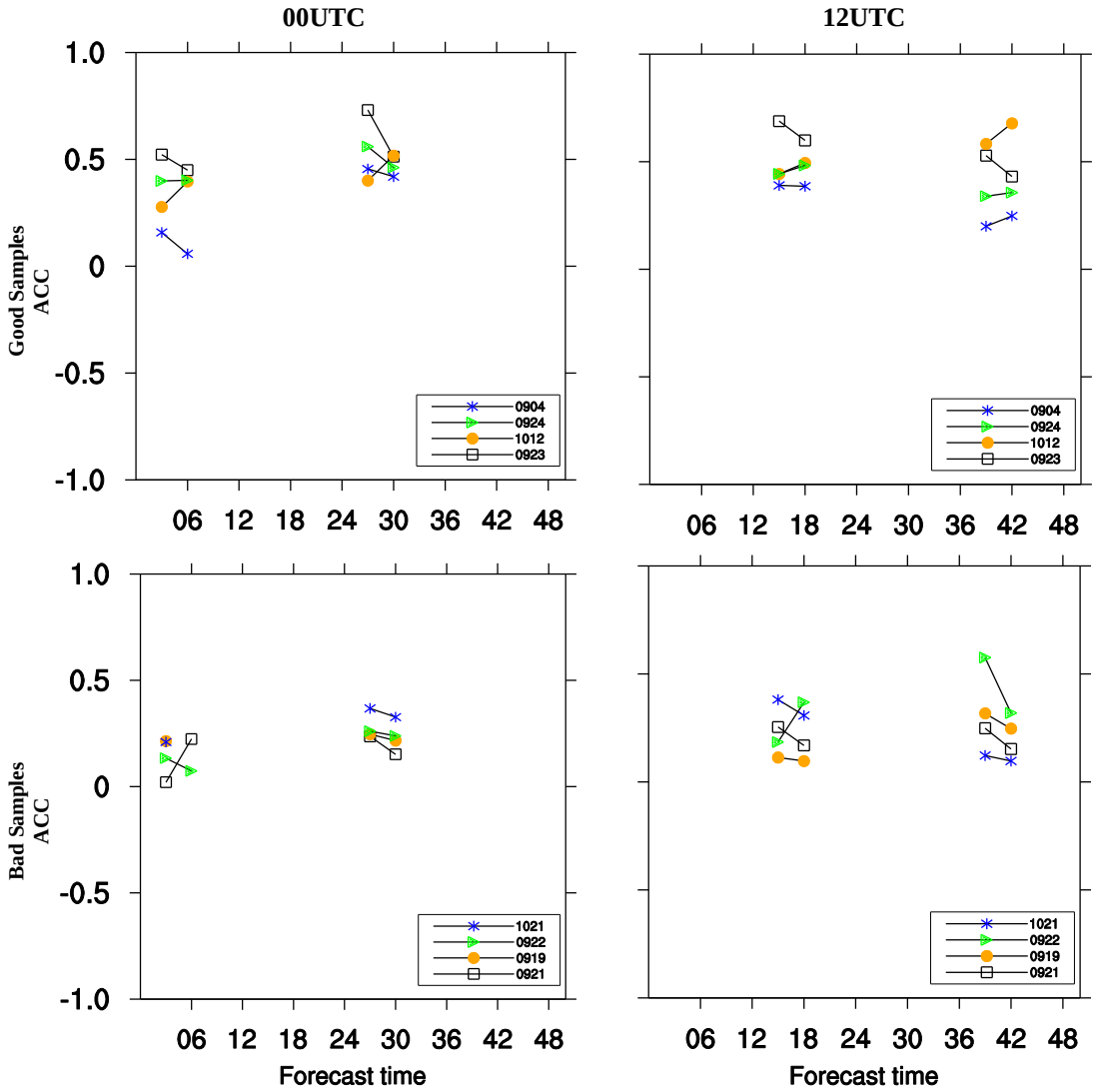

Figure 10. *Time Series of the spatial ACC of cloud water path between the CPEFS model forecasts initialized at 00 (left) /12 (right) UTC and the Himawari-8 observations for cases of good samples (top) and bad samples (bottom) in performance with the forecast lead time*

Discussion and conclusion

This study utilized high-resolution polar-orbiting satellite MODIS cloud products with resolutions of 1 km or 5 km over China Central Region in September and October 2018. By employing the spatial ACC, it objectively analyzed the usability of cloud top temperature and cloud water path products from the Himawari-8 geostationary satellite with the high spatiotemporal resolution over China Central Region. Furthermore, it quantitatively evaluated the cloud field forecasting capability of the next-generation

http://www.aloki.hu ● ISSN 1589 1623 (Print) ● ISSN 1785 0037 (Online)
DOI: http://dx.doi.org/10.15666/aeer/2303_54255441

weather modification model of CPEFS using the Himawari-8 cloud products. The main findings are as follows:

(1) The spatial distribution of cloud top temperature and cloud water path retrieved by the Himawari-8 aligned well with the MODIS retrievals. The spatial ACC between the Himawari-8 and MODIS for cloud top temperature and cloud water path were 0.51–0.67 and 0.68–0.69, respectively. The Himawari-8 effectively identified cold/warm clouds and regions of abundant cloud water.

(2) The cloud observation products from the Himawari-8 with a resolution of 4 km showed the better agreement with the MODIS 5 km cloud observation products, with an improvement in agreement rate of approximately 10% compared to the MODIS 1 km resolution products. The spatial ACC between MODIS (5 km resolution) and Himawari-8 cloud top temperature retrievals ranged from 0.61 to 0.67, whereas for the 1 km MODIS retrievals, it ranged from 0.51 to 0.61.

(3) There were significant case-by-case differences in the spatial distribution agreement of cloud top temperature retrieved by the Himawari-8 and MODIS. In contrast, the spatial distribution agreement for cloud water path showed smaller differences across cases. The maximum spatial ACC for the MODIS-retrieved cloud top temperature compared to the Himawari-8 observations reached 0.85, while the minimum was only 0.40, with the ACC in September being 10% higher than in October. The maximum spatial ACC for the MODIS-retrieved cloud water path compared to the Himawari-8 results reached 0.80, while the minimum was 0.60, with the little difference between September and October.

(4) The spatial ACC for cloud top temperature and cloud water path in China Central Region, as forecasted by the weather modification CPEFS model, were 0.23 and 0.34, respectively, indicating that the forecasting performance required further improvement. Overall, forecasts initiated at 12 UTC showed slightly better performance than those initialized at 00 UTC.

(5) The performance of cloud top temperature forecasts by the CPEFS model exhibited the significant case-specific differences. The spatial ACC between forecasted and observed cloud top temperatures ranged from 0.05 to 0.6 across different cases. In the initial forecast stages, there were large variations in spatial ACC among cases, with 3-hour forecasts showing the spatial ACC between 0 and 0.7. For better-performing cases, rapid adjustments occured during the initialization phase, and performance steadily improved as the forecast lead time increased. In contrast, poorer-performing cases exhibited slower adjustments during initialization, and performance declined with longer forecast lead time.

(6) The performance of cloud water path forecasts by the CPEFS model showed relatively smaller case-specific differences, with the spatial ACC ranging from 0.15 to 0.55 across cases. The initial forecast stage was less reliable, but credibility improved as the forecast lead time increased, followed by a decline in reliability in later stage. For forecasts initialized at 00 UTC, the spatial ACC between 3-6h forecasts of cloud water path and observations ranged from 0 to 0.5. As the forecast lead time increased to 33-36 hours, the spatial ACC for better-performing cases significantly improved, while poorer-performing cases improved more slowly. For forecasts initialized at 12 UTC, the spatial ACC for 15-18h forecasts of cloud water path ranged from 0.1 to 0.7. However, as the lead time increased to 39-42h, the similarity between better-performing case forecasts and observations tended to decline.

http://www.aloki.hu ● ISSN 1589 1623 (Print) ● ISSN 1785 0037 (Online)
DOI: http://dx.doi.org/10.15666/aeer/2303_54255441

In summary, this study utilized the new-generation Himawari-8 geostationary satellite to operationally evaluate the forecast performance of cloud top temperature for the CPEFS model across multiple cases. The results were consistent with previous studies that assessed the performance of cloud top temperature for the CPEFS model using a single case based on the first-generation Fengyun-2 geostationary satellite. Moreover, leveraging the rich cloud products from Himawari-8, this study achieved the operational verification of the forecast performance of cloud water path for the CPEFS model. The evaluation results indicated that the model exhibited better forecasting performance for cloud water path than for cloud-top temperature. By quantitative and real-time operational verification in the forecasting capabilities of the CPEFS in the cloud fields, this research could provide the basis of the reasonable application of model's cloud products in the operational scheme design of weather modification and the optimization of the model's cloud physics scheme.

Acknowledgements. This work was jointly supported by Foundation of China Meteorological Administration Aerosol-Cloud and Precipitation Key Laboratory (Grant No. KDW2405), Foundation of Key Laboratory for Cloud Physics and Weather Modification of China Meteorological Administration (Grant No. 2017Z01608) and Foundation of Jiangsu Meteorological Bureau, China (Grant No. KM201803, KQ202513).

REFERENCES

[1] Ackerman, S. A., Strabala, K. I., Menzel, W. P., Frey, R. A., Moeller, C. C., Gumley, L. E. (1999): Discriminating clear sky from clouds with MODIS. – Journal of Geophysical Research Atmospheres 103 (D24).

[2] Fan, H. J., Huang, Y. P., Li, W. B. (2017): Overview of Retrieval Algorithm of Cloud-Top Height Based on Satellite Infrared Remote Sensing. – Acta Scientiarum Naturalium Universitatis Pekinensis 53(4): 783-792.

[3] Hamada, A., Nishi, N., Iwasaki, S., Ohno, Y., Okamato, H. (2008): Cloud type and top height estimation for tropical upper-tropospheric clouds using GMS-5 split-window measurements combined with cloud radar measurements. – Scientific Online Letters on the Atmosphere Sola 4(1): 57-60.

[4] Li, D., Ding, Y. W., Wei, L., Li, W., Tang, L., Li, Q., Wang, L. (2020): Forecast verification of different weather types in summer and autumn for weather modification model in Hunan Province. – Journal of Meteorological Research and Application 41(2): 50-54.

[5] Liu, Y. B., Ding, Q. J., Shi, Y. Q., Fang, C. G., Duan, J., Lou, X. F., Li, P., Huo, Z. Y., Zhou, Y. B., Wang, H. L., Jing, X. Q., Wang, X., Chen, T. Y., Chen, B. J., Li, J. M. (2021): Development of a cloud-resolvable weather modification model: Model description, preliminary results and challenges. – Advances in Meteorological Science and Technology 11: 77-85.

[6] Ma, Z. S., Liu, Q. J., Qin, Y. Y., Kang, Z. M., Yan, H. (2009): Verification of forecasting efficiency to cloud microphysical characters of mesoscale numerical model for artificial rainfall enhancement by using TRMM satellite data. – Acta Meteorologica Sinica 67(2): 260-271.

[7] Mei, Q., Wang, J., Zhi, X., Zhang, H., Gao, Y., Yi, C., Yang, Y. (2022): Preliminary application of a multi-physical ensemble transform Kalman filter in cloud and precipitation forecasts. – Atmosphere 13: 1359.

[8] Min, M., Wu, C. Q., Li, C., Liu, H., Xu, N., Wu, X., Chen, L., Wang, F., Sun, F., Qin, D. (2017): Developing the science product algorithm testbed for Chinese next-generation

http://www.aloki.hu ● ISSN 1589 1623 (Print) ● ISSN 1785 0037 (Online)
DOI: http://dx.doi.org/10.15666/aeer/2303_54255441

geostationary meteorological satellites: Fengyun-4 series. – Journal of Meteorological Research 31(4): 708-719.

[9] Mouri, K., Suzue, H., Yoshida, R. (2016): Algorithm Theoretical Basis Document for Cloud Top Height Product. – Meteorological Satellite Center Technical Note 61.

[10] Nieman, S. J., Schmetz, J., Menzel, W. P. (1993): A comparison of several techniques to assign heights to cloud tracers. – Journal of Applied Meteorology 32(9): 1559-1568.

[11] Shenk, W. E., Curran, R. J. (1973): A multi-spectral method for estimating cirrus cloud top heights. – Journal of Applied Meteorology 12(7): 1213-1216.

[12] Smith, W. L., Frey, R. (1990): On cloud altitude determinations from high resolution interferometer sounder (HIS) observations. – Journal of Applied Meteorology 29(7): 658-662.

[13] Szejwach, G. (1982): Determination of semi-transparent cirrus cloud temperature from infrared radiances: application to meteosat. – Journal of Applied Meteorology 21(3): 384-393.

[14] Wang, Z., Letu, H., Shang, H., Zhao, C., Li, J., Ma, R. (2019): A supercooled water cloud detection algorithm using Himawari-8 satellite measurements. – Journal of Geophysical Research Atmospheres 124: 2724-2738.

[15] Zhang, P., Guo, Q., Chen, B. Y., Feng, X. (2016): The Chinese next-generation geostationary meteorological satellite FY-4 compared with the Japanese Himawari-8/9 satellites. – Advances in Meteorological Science and Technology 6(1): 72-75.

[16] Zhang, L. P., Zhi, X. F., Wang, J., Wang, Y. H. (2018): Multi-scheme comparative test and ensemble of cloud top height and temperature forecasting. – Meteorological Science Technology 46: 1136-1146.

[17] Zhao, F. S., Sun, T. M., Ding, Q., Kong, Q. X., Hu, W., Xun, S. P., Shao, H. F. (2002): Aniterative algorithm for the retrieval of cloud properties from NOAA-AVHRR imagery. – Meteorological Monthly 60(5): 594-601.

[18] Zhou, Y. Q., Chen, Y. Y., Li, J., Huang, Y. M., He, X. D., Zhou, F. F., Wu, M. X., Hu, B., Mao, J. T. (2008): Retrieval and preliminary text of cloud physical parameters from combination of FY-2C/D geostationary satellite data and other observation data. – Meteorological Monthly 34(12): 27-37.

http://www.aloki.hu ● ISSN 1589 1623 (Print) ● ISSN 1785 0037 (Online)
DOI: http://dx.doi.org/10.15666/aeer/2303_54255441